



Cite this: DOI: 10.1039/d5im00317b

## Investigating the SO<sub>2</sub> absorption behavior of pyrimidine-based deep eutectic solvents *via* a dual-site thermodynamic model

 Yiru Zou,<sup>a,c</sup> Xiaoxiao Xing,<sup>a</sup> Chao Wang,<sup>id</sup> <sup>c</sup> Duanjian Tao,<sup>id</sup> <sup>\*d</sup> Haiyan Ji,<sup>c</sup> Peiwen Wu,<sup>id</sup> <sup>\*c</sup> Yanhong Chao<sup>a</sup> and Wenshuai Zhu<sup>id</sup> <sup>\*abc</sup>

Deep eutectic solvents (DESs), composed of hydrogen bond acceptors (HBAs) and hydrogen bond donors (HBDs), are widely used in flue gas desulfurization due to their excellent SO<sub>2</sub> absorption properties. In this work, 14 DESs with pyrimidine derivatives and their isomers (including 2-aminopyrimidine (AmPyr), 2-chloropyrimidine, 2-bromopyrimidine, 4-amino-2-hydroxypyrimidine, 2,4-dihydroxypyrimidine, 4,6-diaminopyrimidine, 2-aminopyrazine, and 3-aminopyridazine, respectively) as HBDs and 1-ethyl-3-methylimidazolium chloride (C<sub>2</sub>mimCl) and 1-ethyl-3-methylimidazolium bromide as HBAs have been successfully prepared and used for SO<sub>2</sub> absorption. Among them, C<sub>2</sub>mimCl-7 + AmPyr exhibited the highest SO<sub>2</sub> absorption (19.032 mol kg<sup>-1</sup>, at 298.15 K and 1.0 bar), rapid gas-liquid equilibrium within 40 s, and an exceptional ideal selectivity of 528.7 for SO<sub>2</sub>/CO<sub>2</sub>. After 30 cycles of absorption-desorption, the SO<sub>2</sub> absorption capacity remained as high as 18.265 mol kg<sup>-1</sup>. A dual-site reaction equilibrium thermodynamic model (DS-RETM) was established for absorption behavior analysis. Using C<sub>2</sub>mimCl-7 + AmPyr as a case study, Henry's constant, equilibrium constants, and other thermodynamic parameters were determined. DS-RETM fitting further enabled visualization of the potential absorption behavior of each DES component, facilitating comparison of HBA and HBD effects on SO<sub>2</sub> absorption. This study offers new insights into the development of high-performance flue gas desulfurization absorbents and introduces a novel model for thermodynamic analysis of SO<sub>2</sub> absorption in DESs.

 Received 6th November 2025,  
Accepted 5th January 2026

DOI: 10.1039/d5im00317b

[rsc.li/icm](http://rsc.li/icm)

 Keywords: Deep eutectic solvents; SO<sub>2</sub> absorption; Pyrimidine; Thermodynamic; Selectivity.

### 1 Introduction

The various fuels burned in factories during the production process, such as coal, oil, natural gas, *etc.*, will produce a large amount of flue gas.<sup>1</sup> The harmful gases contained therein, especially sulfur dioxide (SO<sub>2</sub>), cause serious damage to the ecological environment and pose a significant threat to human health.<sup>2</sup> In the atmosphere, SO<sub>2</sub> oxidizes into sulfuric acid mist or sulfate aerosols, which are important precursors for environmental acidification. The content of SO<sub>2</sub> exceeding

0.5 ppm has potential impacts on human health, while when its concentration exceeds 1.5 ppm, healthy individuals may suffer from chronic bronchitis, laryngitis, and severe respiratory infections.<sup>3,4</sup> Thus, it is necessary to remove SO<sub>2</sub> before it is released into the atmosphere. Flue gas desulfurization (FGD) is the process of separating SO<sub>2</sub> from flue gas through various technologies and converting it into harmless or usable substances.<sup>5</sup> According to the state of the absorbent and product during the reaction process, it can be divided into wet, dry, and semi-dry desulfurization. Wet desulfurization technology is relatively mature, efficient, and easy to operate, and is the most widely used desulfurization method, including limestone gypsum method, ammonia absorption method, *etc.* However, these traditional absorbents have drawbacks such as irreversibility, volatility, and secondary environmental pollution.<sup>6</sup> Developing efficient, selective, and renewable absorbents is one of the key challenges in FGD technology.

Among all reported efficient absorbents, deep eutectic solvents (DESs) have been regarded as a promising one, because of their high selectivity, remarkable absorption

<sup>a</sup> College of Chemical Engineering and Environment, State Key Laboratory of Heavy Oil Processing, College of Science, China University of Petroleum-Beijing, Beijing 102249, PR China. E-mail: zhuws@cup.edu.cn

<sup>b</sup> Shandong Key Laboratory of Green Electricity & Hydrogen Science and Technology, Shandong Institute of Petroleum and Chemical Technology, Dongying 257061, PR China

<sup>c</sup> School of Chemistry and Chemical Engineering, School of the Environment and Safety Engineering, School of Materials Science and Engineering, Jiangsu University, Zhenjiang 212013, PR China

<sup>d</sup> College of Chemistry and Chemical Engineering, Jiangxi Normal University, Nanchang 330022, PR China



capacity, green characteristics, *etc.*<sup>7</sup> DESs were first proposed by Abbott in 2003 and are widely regarded as one of the green solvents.<sup>8,9</sup> They are formed by the interaction between hydrogen bond donors (HBDs) and hydrogen bond acceptors (HBAs) through hydrogen bonds, halogen bonds, or van der Waals forces, and have advantages such as easy synthesis, recyclability, designability, *etc.*<sup>10–12</sup> Due to the wide variety of HBDs and HBAs, theoretically, there could be at least  $10^6$  types of DESs, which can be designed with specific functions based on application requirements.<sup>13</sup> Since Han *et al.*<sup>14</sup> first used choline chloride-glycerol deep eutectic solvents to absorb  $\text{SO}_2$  in 2013, various DESs have been developed for flue gas desulfurization. Among them, DESs using nitrogen-containing heterocyclic organic compounds as HBDs or HBAs, including imidazole,<sup>15–18</sup> triazole,<sup>19</sup> tetrazole,<sup>20</sup> benzimidazole,<sup>21</sup> pyrazole,<sup>22</sup> pyridine,<sup>23–26</sup> *etc.*, have been reported successively.

Pyrimidine, a six-membered nitrogen-containing heterocyclic organic compound, differs from pyridine in that it contains two alternating N atoms and has lower toxicity. Schröder *et al.*<sup>1</sup> reported that the N atom of the pyrimidine ring can form dipole–dipole interactions with the O atom in  $\text{S}=\text{O}$ , indicating that pyrimidine-based absorbents are excellent candidates for  $\text{SO}_2$  absorption. However, the physical interaction formed by electrostatic attraction between polar molecules is relatively weak, which limits the ability of materials to remove  $\text{SO}_2$ . Notably, DESs prepared from pyridine derivatives containing functional groups such as  $-\text{NH}_2$ ,  $-\text{OH}$ , and  $-\text{COOH}$  exhibit excellent  $\text{SO}_2$  absorption capacity.<sup>25,26</sup> Thus, to prepare pyrimidine-based DESs with high  $\text{SO}_2$  absorption performance, pyrimidine derivatives containing functional groups such as  $-\text{NH}_2$ ,  $\text{C}=\text{O}$ ,  $-\text{Cl}$ , and  $-\text{Br}$  have been inferred to enhance their interactions with  $\text{SO}_2$ .

Previously, to investigate the absorption behavior, the  $\text{SO}_2$  absorption process of DESs was analyzed through a thermodynamic model. Zhang *et al.*<sup>27</sup> obtained the physical and chemical absorption enthalpy changes ( $\Delta_r H_m$ ) of acidic protonic ionic liquid (APIL) based DESs through a reaction equilibrium thermodynamic model (RETM). In our previous work,<sup>28</sup> we also successfully used a RETM to demonstrate that purine-based DESs exhibit chemical absorption in the low-pressure region and physical absorption in the high-pressure region, and obtained a series of thermodynamic parameters. The absorption behavior of different DESs can be observed through the RETM, but how to gain more comprehensive insight into the absorption capacity of each component still needs further exploration.

In this work, a series of DESs with pyrimidine derivatives (one of 2-aminopyrimidine, 2-chloropyrimidine, 2-bromopyrimidine, 4-amino-2-hydroxypyrimidine, 2,4-dihydroxypyrimidine, and 4,6-diaminopyrimidine) or isomers of 2-aminopyrimidine (2-aminopyrazine or 3-aminopyridazine) as HBDs with 1-ethyl-3-methylimidazolium chloride or 1-ethyl-3-methylimidazolium bromide as HBAs have been successfully prepared. The relationship between temperature and the densities as well as viscosities of the prepared DESs was analyzed, and the thermal decomposition temperature ( $T_d$ ) was further determined

through thermogravimetric analysis. Subsequently, the  $\text{SO}_2$  absorption performance of the prepared DESs was measured to investigate the effects of the molar ratio (HBAs:HBDs), HBD type, pressure, and temperature. Moreover, the time-dependent  $\text{SO}_2$  absorption,  $\text{SO}_2/\text{CO}_2$  selectivity and regeneration performance of pyrimidine-based DESs were also explored. Specifically, the physical and chemical absorption behavior of the prepared DESs was investigated using a dual-site reaction equilibrium thermodynamic model (DS-RETM), which can further elucidate the influence of HBAs and HBDs on  $\text{SO}_2$  absorption and thermodynamic parameters. Finally, the possible interaction between pyrimidine-based DESs and  $\text{SO}_2$  was further elucidated. Our findings offer a novel strategy for the design of high-performance, high-selectivity  $\text{SO}_2$  absorbents and introduce a new thermodynamic model for  $\text{SO}_2$  absorption in DESs.

## 2 Results and discussion

### 2.1 Characterization of pyrimidine-based DESs

The densities of the as-prepared DESs with  $\text{C}_2\text{mimCl}$  as a HBA were measured at different temperatures, as shown in Fig. 1a and b (Tables S1 and S2). Obviously, as the molar ratio increases from 2:1 to 7:1, the density of  $\text{C}_2\text{mimCl}-n + \text{AmPyr}$  DESs gradually decreases from  $1.164 \text{ g cm}^{-3}$  to  $1.151 \text{ g cm}^{-3}$  at 298.15 K. Thus, the increase of  $\text{C}_2\text{mimCl}$  is beneficial to decrease the density of  $\text{C}_2\text{mimCl}-n + \text{AmPyr}$  DESs. As for the DESs of  $\text{C}_2\text{mimCl}-7 + \text{HBDs}$ , the order of density (arranged by HBDs) at the same temperature is:  $\text{AmPz} < \text{AmPd} \approx \text{AmPyr} < \text{ChPyr} < \text{DAmPyr} < \text{Cyt} < \text{Ura} < \text{BrPyr}$ . Considering that the molar ratio of  $\text{C}_2\text{mimCl}$  to HBDs remains unchanged, there exists a significant difference in density, indicating that the molecular structure of HBDs will affect the density of DESs significantly.<sup>29</sup> The density of DESs was fitted to the temperature ( $T$ ) ( $\rho_{\text{DESs}} = \alpha + \beta T$ , detailed parameters are provided in Tables S3 and S4). The results show that  $R_1^2$  and  $R_2^2$  are 0.999, revealing a linear relationship between densities and temperatures.

Subsequently, the viscosities of pyrimidine-based DESs were measured at different temperatures, as shown in Fig. 1c and d (Tables S5 and S6). The results in Fig. 1c are similar to the effect of temperature on densities, indicating that increasing  $\text{C}_2\text{mimCl}$  is beneficial for reducing its viscosities, which may be due to the formation of more intramolecular hydrogen bonds.<sup>30,31</sup> In Fig. 1d, the order of viscosities (at 298.15 K) for different  $\text{C}_2\text{mimCl}-7 + \text{HBDs}$  DESs is:  $\text{C}_2\text{mimCl}-7 + \text{BrPyr} < \text{C}_2\text{mimCl}-7 + \text{ChPyr} < \text{C}_2\text{mimCl}-7 + \text{AmPz} < \text{C}_2\text{mimCl}-7 + \text{Ura} < \text{C}_2\text{mimCl}-7 + \text{AmPd} < \text{C}_2\text{mimCl}-7 + \text{AmPyr} < \text{C}_2\text{mimCl}-7 + \text{DAmPyr} < \text{C}_2\text{mimCl}-7 + \text{Cyt}$ . Owing to the different types, positions, and numbers of functional groups in HBDs, their ability to form intramolecular hydrogen bonds with  $\text{C}_2\text{mimCl}$  differs from one another, demonstrating that the structures of HBAs and HBDs significantly alter the viscosities of DESs.<sup>29</sup> In addition, the viscosity of  $\text{C}_2\text{mimCl}-7 + \text{AmPyr}$  is higher than that of  $\text{C}_2\text{mimBr}-7 + \text{AmPyr}$ , which may be due to the



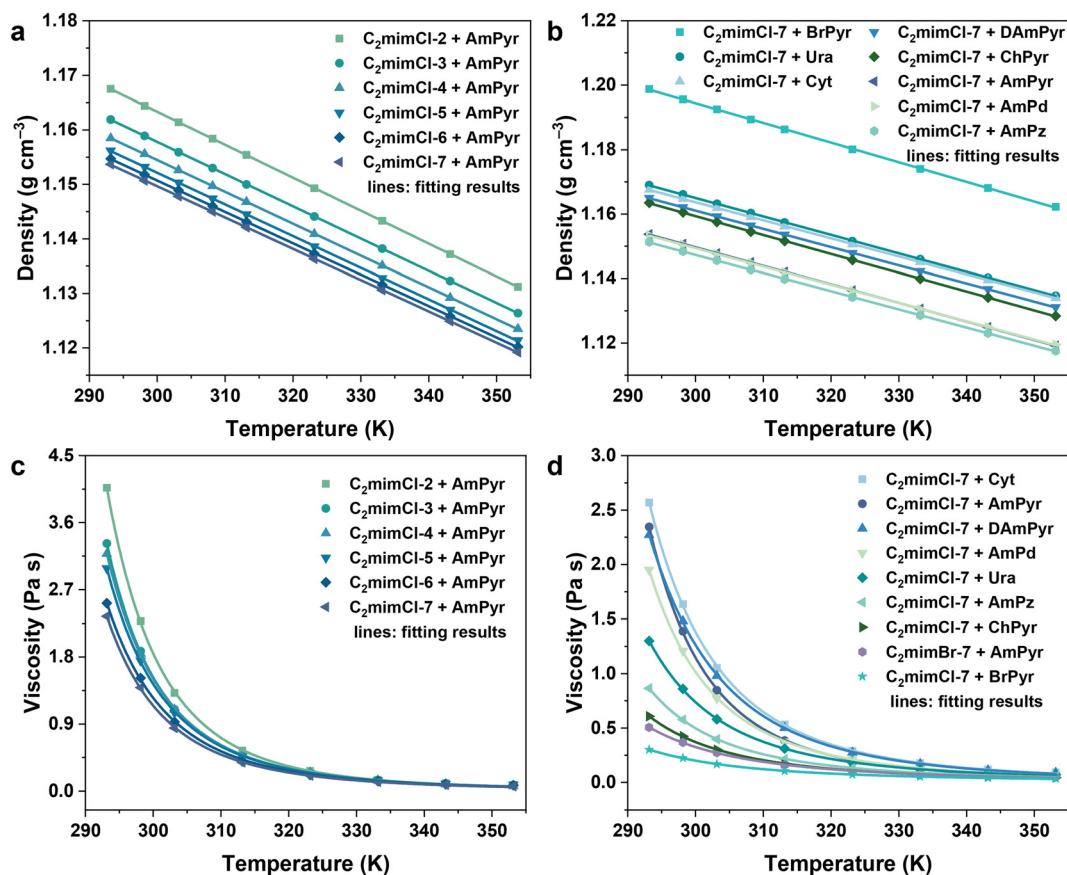


Fig. 1 The densities of (a)  $C_2mimCl-n + AmPyr$  ( $n = 2, 3, 4, 5, 6, 7$ ) and (b)  $C_2mimCl-7 + HBDs$ ; the viscosities of (c)  $C_2mimCl-n + AmPyr$  ( $n = 2, 3, 4, 5, 6, 7$ ) and (d) HBAs-7 + HBDs.

different anions of HBAs, leading to the weaker ability of  $C_2mimBr$  and  $AmPyr$  to form intermolecular hydrogen bonds.<sup>32</sup> The viscosities were fitted to the temperature ( $T$ ) (VFT equation:  $\eta = \eta_0 \exp(t/(T - T_0))$ ),<sup>33</sup> and the detailed parameter data are shown in Tables S7 and 1). The results indicate that  $R_3^2$  and  $R_4^2$  are 0.999, suggesting an exponential relationship between viscosities and temperatures.

To investigate the thermal stability of pyrimidine-based DESs, HBAs-7 + HBDs were analyzed by thermogravimetry (TG), as shown in Fig. S1 and Table 1. Thermal decomposition temperature ( $T_d$ ) can be used to judge the absorption temperature of absorbent and desorption

temperature during regeneration, which is generally defined as the temperature at which the mass loss exceeds 5%. The maximum  $T_d$  value is 519 K ( $C_2mimCl-7 + AmPz$ ), and the minimum value is 393 K ( $C_2mimCl-7 + BrPyr$ ), indicating that pyrimidine-based DESs have excellent thermal stability during absorption–desorption processes and have the potential for flue gas desulfurization at high temperature.

## 2.2 $SO_2$ absorption of pyrimidine-based DESs

To explore the optimal molar ratio of HBAs to HBDs, the  $SO_2$  absorption capacity of  $C_2mimCl-n + AmPyr$  was

Table 1 The viscosity fitting results and  $T_d$  of  $C_2mimCl-7 + HBDs$

Parameters	HBDs								
	Cyt	AmPyr	DAmPyr	AmPd	Ura	AmPz	ChPyr	AmPyr*	BrPyr
$\eta_0 \times 10^4$ (Pa s)	6.591 ± 3.095	5.847 ± 2.319	4.233 ± 1.846	9.167 ± 3.933	13.50 ± 4.797	15.90 ± 3.597	12.20 ± 2.858	14.00 ± 8.586	18.60 ± 4.826
$t_2$ (K)	696.7 ± 83.61	601.2 ± 59.98	800.0 ± 85.88	563.1 ± 66.87	522.0 ± 58.61	448.2 ± 35.34	492.1 ± 41.15	495.7 ± 115.5	396.2 ± 46.08
$T_0$ (K)	208.9 ± 5.231	220.7 ± 3.644	200.0 ± 5.216	219.7 ± 4.482	217.2 ± 4.495	222.0 ± 2.981	214.0 ± 3.567	209.1 ± 10.69	215.4 ± 5.018
$R_4^2$	0.999	0.999	0.999	0.999	0.999	0.999	0.999	0.999	0.999
$T_d$ (K)	508	443	503	514	503	519	464	444	393

AmPyr\*:  $C_2mimBr-7 + AmPyr$ .



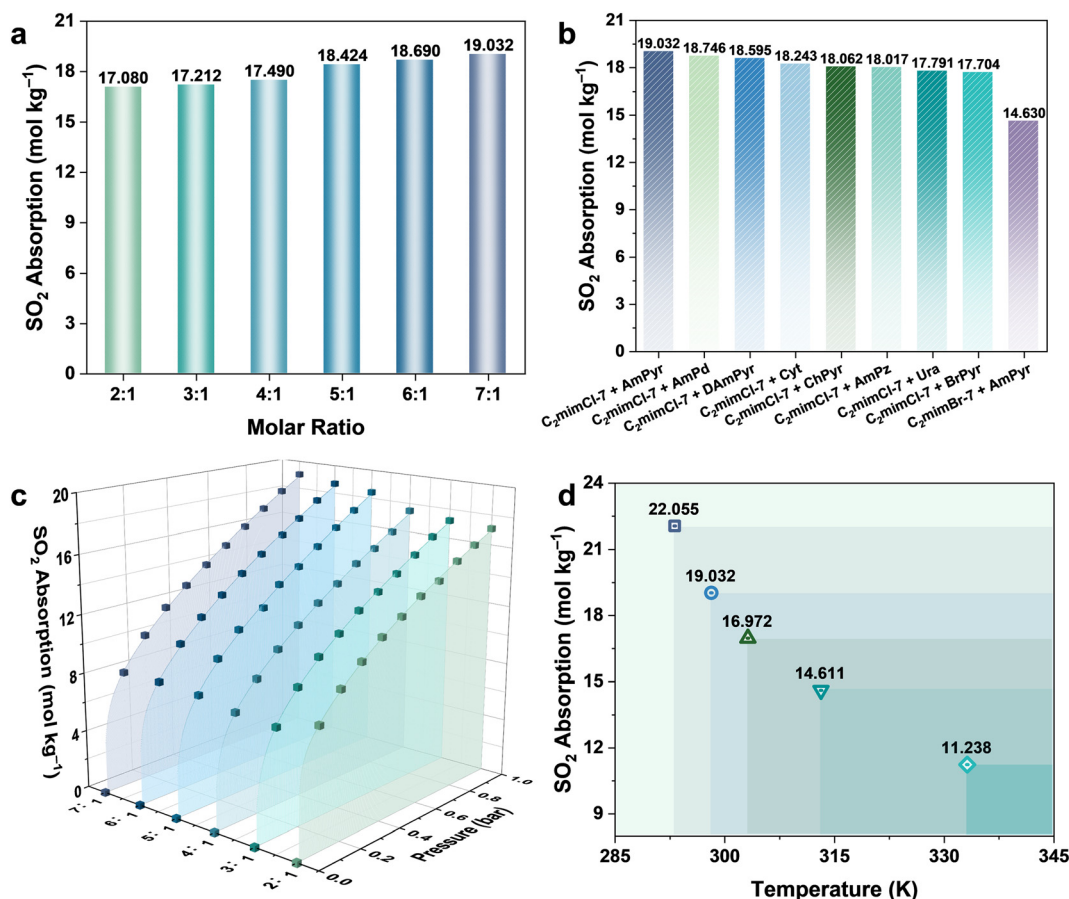


Fig. 2 The SO<sub>2</sub> absorption of (a) C<sub>2</sub>mimCl-*n* + AmPyr and (b) HBAs-7 + HBDs, *T* = 298.15 K, *P* = 1.0 bar; (c) the effect of pressure on SO<sub>2</sub> absorption of C<sub>2</sub>mimCl-*n* + AmPyr, *T* = 298.15 K; (d) the effect of temperature on SO<sub>2</sub> absorption of C<sub>2</sub>mimCl-7 + AmPyr; *P* = 1.0 bar.

investigated. Fig. 2a shows the SO<sub>2</sub> absorption of C<sub>2</sub>mimCl-*n* + AmPyr at 298.15 K and 1.0 bar. As the molar ratio of C<sub>2</sub>mimCl to AmPyr increases, the SO<sub>2</sub> absorption of C<sub>2</sub>mimCl-*n* + AmPyr increases gradually, reaching a maximum of 19.032 mol kg<sup>-1</sup>. With the increase of C<sub>2</sub>mimCl, the viscosity of C<sub>2</sub>mimCl-*n* + AmPyr decreases, which is more beneficial to mass transfer;<sup>34</sup> nevertheless, the charge-transfer interaction between the highly electronegative Cl<sup>-</sup> in C<sub>2</sub>mimCl and the S atoms in SO<sub>2</sub> (Cl<sup>-</sup>⋯SO<sub>2</sub>) is beneficial for improving SO<sub>2</sub> absorption.<sup>35,36</sup> According to the above analysis, the optimal molar ratio of C<sub>2</sub>mimCl to AmPyr is 7:1.

Furthermore, a series of HBAs-7 + HBDs DESs were synthesized, and their SO<sub>2</sub> absorption capacity is shown in Fig. 2b. Besides, Table S8 shows the SO<sub>2</sub> absorption capacity of synthesized DESs compared to other materials, which are superior to many solid absorbents. For DESs with different HBAs, the absorption capacity of C<sub>2</sub>mimBr-7 + AmPyr (14.630 mol kg<sup>-1</sup>) is significantly lower compared to C<sub>2</sub>mimCl-7 + AmPyr (19.032 mol kg<sup>-1</sup>), indicating that anions have a greater influence on SO<sub>2</sub> absorption capacity. In other words, the greater the electronegativity, the higher the absorption capacity of SO<sub>2</sub>.<sup>29,32</sup> As isomers of AmPyr, AmPd and AmPz were also used to form DESs with C<sub>2</sub>mimCl. The SO<sub>2</sub>

absorption capacities of C<sub>2</sub>mimCl-7 + AmPz and C<sub>2</sub>mimCl-7 + AmPd are 18.017 mol kg<sup>-1</sup> and 18.746 mol kg<sup>-1</sup>, respectively. These values, all lower than that of C<sub>2</sub>mimCl-7 + AmPyr (19.032 mol kg<sup>-1</sup>), demonstrate that the position of the nitrogen atoms within the heterocyclic ring structure of the HBDs also significantly impacts the performance of DESs, and the pyrimidine ring is more conducive to SO<sub>2</sub> absorption.

Hence, to develop pyrimidine-based DESs with superior performance, the SO<sub>2</sub> absorption of DESs using pyrimidine derivatives with different functional groups as HBDs was investigated. Firstly, with BrPyr, ChPyr, and AmPyr as HBDs, the SO<sub>2</sub> absorption capacity is C<sub>2</sub>mimCl-7 + BrPyr < C<sub>2</sub>mimCl-7 + ChPyr < C<sub>2</sub>mimCl-7 + AmPyr. Typically, the higher the viscosity, the smaller the absorption capacity. Here, the main reason that affects the absorption capacity is that AmPyr contains weak basic functional groups (-NH<sub>2</sub>), which may have acid-base interaction with SO<sub>2</sub> molecules.<sup>37</sup> Then, the SO<sub>2</sub> absorption of DESs with multifunctional pyrimidine derivatives (Ura, Cyt, and DAmPyr) as HBDs was further investigated. The SO<sub>2</sub> absorption of the three DESs is C<sub>2</sub>mimCl-7 + Ura (17.791 mol kg<sup>-1</sup>) < C<sub>2</sub>mimCl-7 + Cyt (18.243 mol kg<sup>-1</sup>) < C<sub>2</sub>mimCl-7 + DAmPyr (18.595 mol kg<sup>-1</sup>). Thus, the pyrimidine-based DESs with optimal SO<sub>2</sub> absorption is C<sub>2</sub>mimCl-7 + AmPyr.



It is universally known that pressure plays a key role in affecting the gas absorption capacity of DESs.<sup>38</sup> Fig. 2c shows the SO<sub>2</sub> absorption of pyrimidine-based DESs at 298.15 K and 0–1.0 bar. The SO<sub>2</sub> absorption capacity of C<sub>2</sub>mimCl-*n* + AmPyr increases nonlinearly with the increase of pressure. Taking C<sub>2</sub>mimCl-7 + AmPyr with the highest absorption capacity as an example, with the pressure increasing from 0.1 bar to 1.0 bar, the absorption capacity of SO<sub>2</sub> increases from 7.911 mol kg<sup>-1</sup> to 19.032 mol kg<sup>-1</sup>. This shows that increasing the pressure can promote the absorption of SO<sub>2</sub>. Conversely, reducing the pressure can be considered to desorb SO<sub>2</sub>.<sup>39,40</sup> Additionally, the SO<sub>2</sub> absorption increases rapidly between 0 and 0.1 bar, probably owing to the chemical interaction between the absorbent and SO<sub>2</sub> molecules.<sup>41</sup> However, the growth rate of absorption capacity decreases between 0.1 and 1.0 bar, which may be due to the gradual occupation of absorption sites, so rapid absorption has been completed, resulting in the process being dominated by physical absorption. Therefore, it is speculated that the absorption process of SO<sub>2</sub> via pyrimidine-based DESs includes chemical absorption and physical absorption.<sup>42</sup>

According to the existing literature,<sup>6,22,43–46</sup> temperature is another important factor affecting the absorption capacity of DESs. Hence, C<sub>2</sub>mimCl-7 + AmPyr was selected to investigate the SO<sub>2</sub> absorption performance at different temperatures, as shown in Fig. 2d. With the increase of temperature, the SO<sub>2</sub> absorption capacity of C<sub>2</sub>mimCl-7 + AmPyr decreases continuously, and the absorption capacities are 22.055, 19.032, 16.972, 14.611 and 11.238 mol kg<sup>-1</sup>, respectively. This result shows that increasing the temperature is beneficial to the regeneration of absorbent. Furthermore, it should be noted that C<sub>2</sub>mimCl-7 + AmPyr still has a high absorption capacity at high temperatures, indicating that pyrimidine-based DESs could be used as candidate absorbents for high-temperature flue gas desulfurization.<sup>29</sup>

### 2.3 Analysis of SO<sub>2</sub> absorption behavior for pyrimidine-based DESs

A DS-RETM equation was established for fitting the SO<sub>2</sub> absorption.<sup>47</sup> It is assumed that the absorption of SO<sub>2</sub> by C<sub>2</sub>mimCl-7 + AmPyr DESs involves the following steps:



where g and l stand for gaseous and liquid states, respectively. C<sub>2</sub>mimCl-SO<sub>2</sub> stands for the interaction of C<sub>2</sub>mimCl with SO<sub>2</sub>, and AmPyr-SO<sub>2</sub> stands for the interaction of AmPyr with SO<sub>2</sub>. Eqn (1) denotes the physical absorption process and could be described by the following equation:

$$P = H \cdot \gamma_{\text{SO}_2} \cdot \frac{m_{\text{phys-SO}_2}}{m^\circ} \quad (4)$$

where *P* is the pressure (bar) of SO<sub>2</sub> (g); *H* is the Henry's law constant with the same unit as *P*; *m*<sub>phys-SO<sub>2</sub></sub> is the physical absorption molality (mol kg<sup>-1</sup>);  $\gamma_{\text{SO}_2}$  is the activity coefficient; *m*<sup>o</sup> is 1.0 mol kg<sup>-1</sup>. Eqn (2) and (3) denote the chemical absorption process and could be described by following equations:

$$k_{\text{C}_2\text{mimCl}} = \frac{\gamma_{\text{C}_2\text{mimCl-SO}_2} \cdot \frac{m_{\text{C}_2\text{mimCl-SO}_2}}{m^\circ}}{\frac{P}{P^\circ} \cdot \gamma_{\text{C}_2\text{mimCl}} \cdot \frac{m_{\text{C}_2\text{mimCl}}}{m^\circ}} \quad (5)$$

$$m_{\text{C}_2\text{mimCl}}^\circ = m_{\text{C}_2\text{mimCl-SO}_2} + m_{\text{C}_2\text{mimCl}} \quad (6)$$

$$k_{\text{AmPyr}} = \frac{\gamma_{\text{AmPyr-SO}_2} \cdot \frac{m_{\text{AmPyr-SO}_2}}{m^\circ}}{\frac{P}{P^\circ} \cdot \gamma_{\text{AmPyr}} \cdot \frac{m_{\text{AmPyr}}}{m^\circ}} \quad (7)$$

$$m_{\text{AmPyr}}^\circ = m_{\text{AmPyr-SO}_2} + m_{\text{AmPyr}} \quad (8)$$

$$m_{\text{C}_2\text{mimCl}}^\circ = \frac{1}{M_{\text{C}_2\text{mimCl}}} \quad (9)$$

$$m_{\text{AmPyr}}^\circ = \frac{1}{M_{\text{AmPyr}}} \quad (10)$$

where *k*<sub>C<sub>2</sub>mimCl</sub> and *k*<sub>AmPyr</sub> stand for the equilibrium constants;  $\gamma_{\text{C}_2\text{mimCl-SO}_2}$ ,  $\gamma_{\text{C}_2\text{mimCl}}$ ,  $\gamma_{\text{AmPyr-SO}_2}$ , and  $\gamma_{\text{AmPyr}}$  are the activity coefficients; *m*<sub>C<sub>2</sub>mimCl-SO<sub>2</sub></sub>, *m*<sub>C<sub>2</sub>mimCl</sub>, *m*<sub>AmPyr-SO<sub>2</sub></sub>, and *m*<sub>AmPyr</sub> are the molality (mol kg<sup>-1</sup>); *P*<sup>o</sup> is 1.0 bar; *m*<sub>C<sub>2</sub>mimCl</sub><sup>o</sup> and *m*<sub>AmPyr</sub><sup>o</sup> are constants (mol kg<sup>-1</sup>) that could be calculated using eqn (9) and (10); *M*<sub>C<sub>2</sub>mimCl</sub> and *M*<sub>AmPyr</sub> are the molar mass of C<sub>2</sub>mimCl and AmPyr, respectively, in g mol<sup>-1</sup>.

The values of  $\gamma_{\text{SO}_2}$ ,  $\gamma_{\text{C}_2\text{mimCl-SO}_2}$ ,  $\gamma_{\text{C}_2\text{mimCl}}$ ,  $\gamma_{\text{AmPyr-SO}_2}$ , and  $\gamma_{\text{AmPyr}}$  are all regarded as 1.0.<sup>28,48</sup> Thus, the DS-RETM could be expressed by eqn (11) and (12):

$$m_t = m_{\text{phys-SO}_2} + m_{\text{C}_2\text{mimCl-SO}_2} + m_{\text{AmPyr-SO}_2} \quad (11)$$

$$m_t = \frac{P}{H} + \frac{k_{\text{C}_2\text{mimCl}} \cdot P \cdot m_{\text{C}_2\text{mimCl}}^\circ}{k_{\text{C}_2\text{mimCl}} \cdot P + 1} + \frac{k_{\text{AmPyr}} \cdot P \cdot m_{\text{AmPyr}}^\circ}{k_{\text{AmPyr}} \cdot P + 1} \quad (12)$$

where *m*<sub>t</sub> (mol kg<sup>-1</sup>) is the total SO<sub>2</sub> absorption.

The SO<sub>2</sub> absorption of C<sub>2</sub>mimCl-7 + AmPyr at different temperatures and pressures was correlated according to eqn (12), and fitted lines are shown in Fig. 3a. Notably, the fitting curve matches well with the experimental data, with *R*<sub>5</sub><sup>2</sup> values greater than 0.999, indicating that the established thermodynamic model has extremely high reliability. The corresponding fitting parameters were calculated and revealed in Table 2. The Henry's law constants keep an increasing trend, while the equilibrium constants keep a decreasing trend, which is consistent with the negative dependence of SO<sub>2</sub> absorption on temperature.

Based on the *H*, *k*<sub>C<sub>2</sub>mimCl</sub>, and *k*<sub>AmPyr</sub>, the *m*<sub>phys-SO<sub>2</sub></sub>, *m*<sub>C<sub>2</sub>mimCl-SO<sub>2</sub></sub> and *m*<sub>AmPyr-SO<sub>2</sub></sub> could be obtained. As shown in Fig. 3b and c, both physical absorption and chemical absorption decrease with increasing temperature. The



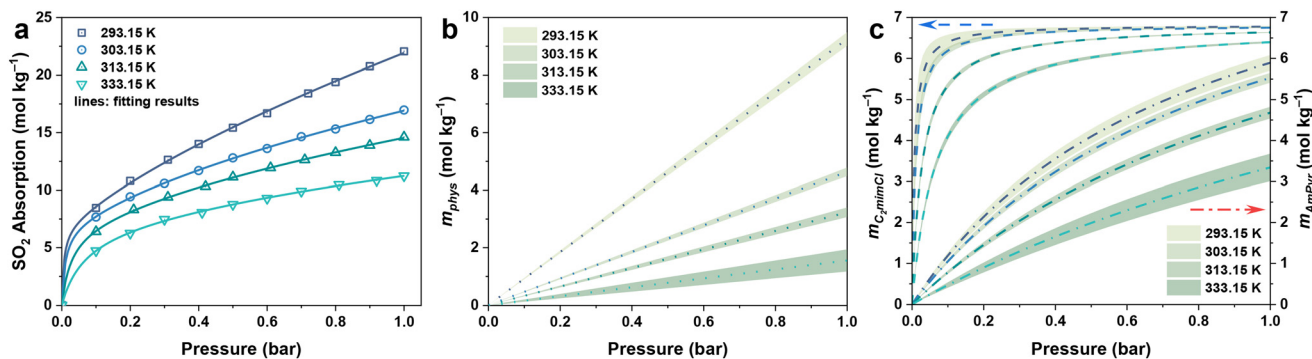


Fig. 3 (a) DS-DETM equation fitting of  $C_2mimCl-7 + AmPyr$  for  $SO_2$  absorption; the calculated (b) physical and (c) chemical absorption of  $SO_2$  by  $C_2mimCl-7 + AmPyr$ .

Table 2 Calculated Henry's law constants, reaction equilibrium constants, and thermodynamic parameters of  $SO_2$  absorption in  $C_2mimCl-7 + AmPyr$  DESs

Parameters	293.15 K	303.15 K	313.15 K	333.15 K
$H$ (bar)	$0.10814 \pm 0.00279$	$0.21585 \pm 0.00688$	$0.30983 \pm 0.01596$	$0.66939 \pm 0.16117$
$k_{C_2mimCl}$	$173.03801 \pm 72.62040$	$99.15970 \pm 14.25614$	$36.28764 \pm 2.19755$	$15.10983 \pm 0.82593$
$k_{AmPyr}$	$1.27796 \pm 0.09255$	$1.11052 \pm 0.05036$	$0.80265 \pm 0.04400$	$0.46775 \pm 0.06859$
$R_5^2$	0.999	0.999	0.999	0.999
$\Delta_{phys}H_m$ (kJ mol $^{-1}$ )	-35.993	-35.993	-35.993	-35.993
$\Delta_{phys}G_m$ (kJ mol $^{-1}$ )	-5.421	-3.864	-3.051	-1.112
$\Delta_{phys}S_m$ (J mol K $^{-1}$ )	-104.287	-105.983	-105.197	-104.701
$\Delta_{chem}H_m$ (kJ mol $^{-1}$ )	-72.131	-72.131	-72.131	-72.131
$\Delta_{chem}G_m$ (kJ mol $^{-1}$ )	-13.158	-11.850	-8.779	-5.416
$\Delta_{chem}S_m$ (J mol K $^{-1}$ )	-201.169	-198.85	-202.308	-200.254
$\Delta_rH_m$ (kJ mol $^{-1}$ )	-108.124	-108.124	-108.124	-108.124
$\Delta_rG_m$ (kJ mol $^{-1}$ )	-18.579	-15.714	-11.829	-6.528
$\Delta_rS_m$ (J mol K $^{-1}$ )	-305.457	-304.833	-307.505	-304.955

$m_{phys-SO_2}$  is most significantly controlled by temperature, followed by  $m_{AmPyr-SO_2}$ , and  $m_{C_2mimCl-SO_2}$  is least affected, indicating that the interaction between  $C_2mimCl$  and  $SO_2$  is stronger than  $AmPyr$ , and the physical interaction is the weakest. Besides, the physical absorption capacity increases linearly with increasing pressure, while the chemical absorption capacity increases nonlinearly and

gradually approaches equilibrium. Thus, the absorption capacity of DESs for  $SO_2$  gradually increases linearly with the increase of pressure.

According to the relationship of  $\ln H$  and  $\ln k$  to  $1/T$  (Fig. 4a), the parameters of enthalpy change ( $\Delta H_m$ ), Gibbs free energy change ( $\Delta G_m$ ), and entropy change ( $\Delta S_m$ ) could be obtained by the following equations:

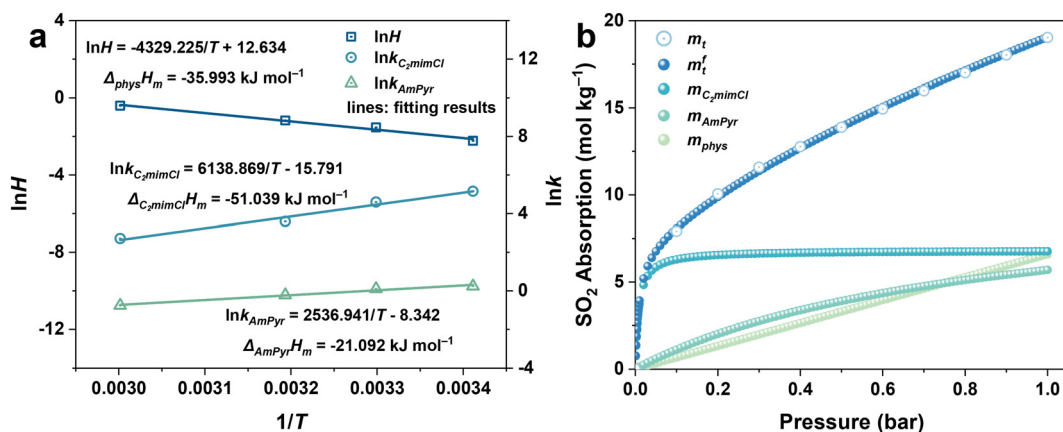


Fig. 4 (a) The fitting results of  $\ln H$  and  $\ln k$  to  $1/T$  of  $C_2mimCl-7 + AmPyr$ ; (b) the calculated  $SO_2$  absorption of  $C_2mimCl-7 + AmPyr$  at 298.15 K.



$$\Delta_{\text{phys}}H_m = R \left( \frac{\partial \ln H_m}{\partial (1/T)} \right) \quad (13)$$

$$\Delta_{\text{phys}}G_m = RT \ln H_m \quad (14)$$

$$\Delta_{\text{phys}}S_m = \frac{\Delta_{\text{phys}}H_m - \Delta_{\text{phys}}G_m}{T} \quad (15)$$

$$\Delta_{\text{C}_2\text{mimCl}}H_m = -R \left( \frac{\partial \ln k_{\text{C}_2\text{mimCl}}}{\partial (1/T)} \right) \quad (16)$$

$$\Delta_{\text{AmPyr}}H_m = -R \left( \frac{\partial \ln k_{\text{AmPyr}}}{\partial (1/T)} \right) \quad (17)$$

$$\Delta_{\text{chem}}H_m = \Delta_{\text{C}_2\text{mimCl}}H_m + \Delta_{\text{AmPyr}}H_m \quad (18)$$

$$\Delta_{\text{chem}}G_m = -RT(\ln k_{\text{C}_2\text{mimCl}} + \ln k_{\text{AmPyr}}) \quad (19)$$

$$\Delta_{\text{chem}}S_m = \frac{\Delta_{\text{chem}}H_m - \Delta_{\text{chem}}G_m}{T} \quad (20)$$

Here,  $\Delta_{\text{phys}}H_m$ ,  $\Delta_{\text{phys}}G_m$ , and  $\Delta_{\text{phys}}S_m$  correspond to the physical process;  $\Delta_{\text{C}_2\text{mimCl}}H_m$ ,  $\Delta_{\text{AmPyr}}H_m$ ,  $\Delta_{\text{chem}}H_m$ ,  $\Delta_{\text{chem}}G_m$ , and  $\Delta_{\text{chem}}S_m$  correspond to the chemical process (Table 2). As can be seen, the values of  $\Delta H_m$ ,  $\Delta G_m$ , and  $\Delta S_m$  are always less than 0, which indicate the absorption process is exothermic, spontaneous, and with increased orderliness.

Besides, the  $\ln H$ ,  $\ln k_{\text{C}_2\text{mimCl}}$ , and  $\ln k_{\text{AmPyr}}$  at 298.15 K can be calculated, and the  $\text{SO}_2$  absorption of  $m_{\text{phys}}$ ,  $m_{\text{C}_2\text{mimCl}}$ ,  $m_{\text{AmPyr}}$ , and  $m_t^f$  could be further obtained. Fig. 4b shows that the calculated  $\text{SO}_2$  absorption remains consistent with the experimental values (such as 19.051 mol kg<sup>-1</sup> vs. 19.032 mol kg<sup>-1</sup> at 1.0 bar), indicating the high reliability of the DS-RETM equation.

To further investigate the absorption behavior of different pyrimidine-based DESs,  $m_{\text{C}_2\text{mimCl}}^0$  and  $m_{\text{AmPyr}}^0$  in eqn (12) were replaced with the initial molality of the corresponding HBAs and HBDs ( $m_{\text{HBAs}}^0$  and  $m_{\text{HBDs}}^0$ ), resulting in DS-RETM equations for different HBAs-7 + HBDs DESs. Subsequently, the  $\text{SO}_2$  absorption of different pyrimidine-based DESs at 298.15 K was fitted, and the detailed results are shown in Fig. S2 and Table S9. Based on the obtained  $H$ ,  $k_{\text{HBAs}}$ , and  $k_{\text{HBDs}}$ , the  $m_{\text{phys}}$ ,  $m_{\text{HBAs}}$ , and  $m_{\text{HBDs}}$  of corresponding HBAs-7 + HBDs DESs could be calculated separately, which is of great significance for insight exploration of the absorption behavior of each component in DESs (Fig. S3). Compared with  $\text{C}_2\text{mimBr-7} + \text{AmPyr}$ , the  $m_{\text{HBDs}}$ ,  $m_{\text{HBAs}}$ , and  $m_{\text{phys}}$  of  $\text{C}_2\text{mimCl-7} + \text{AmPyr}$  were significantly increased, indicating that Cl<sup>-</sup> has a key impact on the  $\text{SO}_2$  absorption of DESs. Obviously, for DESs using the same HBAs ( $\text{C}_2\text{mimCl-7} + \text{HBDs}$ ), there is not much difference in  $m_{\text{HBAs}}$  (also known as  $m_{\text{C}_2\text{mimCl}}$ ) (Fig. S3a and b), attributed to the same molar mass of  $\text{C}_2\text{mimCl}$ , which forms a strong charge transfer interaction between Cl<sup>-</sup> and the S atom of  $\text{SO}_2$  (Cl<sup>-</sup>⋯ $\text{SO}_2$ ). However, significant differences in  $m_{\text{HBDs}}$  and  $m_{\text{phys}}$  between  $\text{C}_2\text{mimCl-7} + \text{HBDs}$

DESs could be observed. Notably, the order of  $m_{\text{HBDs}}$  is not the same as the  $\text{SO}_2$  absorption of their corresponding DESs (Fig. S3c and d). Among them,  $m_{\text{AmPd}}$  and  $m_{\text{DAmPyr}}$  are both greater than  $m_{\text{AmPyr}}$ , but the  $\text{SO}_2$  absorption of  $\text{C}_2\text{mimCl-7} + \text{AmPyr}$  is greater than that of  $\text{C}_2\text{mimCl-7} + \text{AmPd}$  and  $\text{C}_2\text{mimCl-7} + \text{DAmPyr}$ . Interestingly, for the physical absorption ( $m_{\text{phys}}$ ) of  $\text{C}_2\text{mimCl-7} + \text{HBDs}$  (Fig. S3e and f), there is even a phenomenon opposite to the  $\text{SO}_2$  absorption of the corresponding DESs. For instance,  $\text{C}_2\text{mimCl-7} + \text{BrPyr}$  has the minimum  $\text{SO}_2$  absorption but the maximum  $m_{\text{phys}}$ . To sum up, the types and numbers of functional groups in HBDs determine their varying abilities to absorb  $\text{SO}_2$ , while also affecting the physical absorption properties of the corresponding DESs. Hence, DS-RETM fitting could visualize these potential absorption behaviors, which is more conducive to exploring the physical and chemical absorption processes of the prepared DESs.

#### 2.4 Kinetic analysis of $\text{SO}_2$ absorption for pyrimidine-based DESs

A typical time-dependent  $\text{SO}_2$  absorption process involves taking a certain amount of DESs (~0.10 g) and observing the change in  $\text{SO}_2$  absorption capacity over time at an initial pressure of ~1.0 bar. The time-dependent  $\text{SO}_2$  absorption capacity of  $\text{C}_2\text{mimCl-7} + \text{HBDs}$  at 298.15 K is shown in Fig. 5a. Interestingly, the as-prepared DESs can absorb  $\text{SO}_2$  rapidly, which suggests that the absorption process is mainly dominated by chemical absorption. To further observe the  $\text{SO}_2$  absorption rate, Boltzmann equation (eqn (21)) fitting was performed on the experimental results,<sup>32</sup> and the first derivative of the curve is the absorption rate of the as-prepared pyrimidine-based DESs (Fig. 5b). Clearly,  $\text{C}_2\text{mimCl-7} + \text{AmPyr}$  achieved the maximum absorption rate in the shortest possible time. Moreover, the as-prepared DESs can rapidly absorb  $\text{SO}_2$  and basically achieve absorption equilibrium within 40 s, which is superior to numerous reported DESs.<sup>35,49–51</sup> This result shows that pyrimidine-based DESs have potential for flue gas desulfurization.

$$m_{\text{SO}_2} = \frac{A_1 - A_2}{1 + e^{(t-t_0)/d_t}} + A_2 \quad (21)$$

where  $m_{\text{SO}_2}$  refers to the  $\text{SO}_2$  absorption capacity (mol kg<sup>-1</sup>),  $t$  refers to the time of  $\text{SO}_2$  absorption (s), and  $A_1$ ,  $A_2$ ,  $t_0$ , and  $d_t$  refer to the empirical constants.

#### 2.5 $\text{SO}_2/\text{CO}_2$ absorption selectivity of pyrimidine-based DESs

Owing to the complex composition of actual flue gas, it generally contains 0.04–15%  $\text{CO}_2$ .<sup>52</sup> Thus, the designed absorbent for flue gas desulfurization should have high  $\text{SO}_2/\text{CO}_2$  selectivity. The  $\text{CO}_2$  and  $\text{SO}_2$  absorption capacities of  $\text{C}_2\text{mimCl-7} + \text{HBDs}$  were compared at 298.15 K and 1.0 bar, as shown in Fig. 6. Obviously, pyrimidine-based DESs show a negative absorption of  $\text{CO}_2$ . Generally, the selectivity of  $\text{SO}_2/\text{CO}_2$  keeps the ratio of  $\text{SO}_2$  absorption capacity to  $\text{CO}_2$  absorption capacity under given conditions



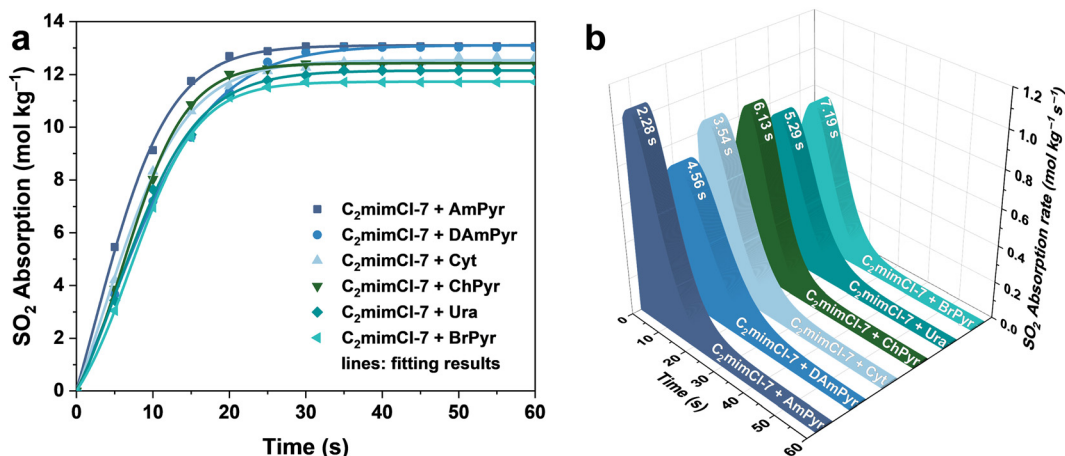


Fig. 5 (a) The time-dependent  $\text{SO}_2$  absorption and (b)  $\text{SO}_2$  absorption rate of pyrimidine-based DESs;  $T = 298.15 \text{ K}$ .

( $S_{\text{DESs}} = m_{\text{SO}_2}/m_{\text{CO}_2}$ ).<sup>29</sup> The comparison of  $\text{SO}_2$  absorption capacity and selectivity with literature data is shown in Table S10. Accordingly, the absorption selectivity of pyrimidine-based DESs is  $\text{C}_2\text{mimCl-7} + \text{ChPyr}$  (451.6),  $\text{C}_2\text{mimCl-7} + \text{Ura}$  (494.2),  $\text{C}_2\text{mimCl-7} + \text{AmPyr}$  (528.7),  $\text{C}_2\text{mimCl-7} + \text{BrPyr}$  (536.5),  $\text{C}_2\text{mimCl-7} + \text{DAmPyr}$  (808.5),  $\text{C}_2\text{mimCl-7} + \text{Cyt}$  (1073.1), respectively. The minimum value of  $S_{\text{DESs}}$  has reached up to 451.6, indicating that pyrimidine-based DESs have excellent  $\text{SO}_2/\text{CO}_2$  selective absorption performance and could be used as a candidate for selective absorption of  $\text{SO}_2$  from actual flue gas.

## 2.6 $\text{SO}_2$ absorption mechanism of pyrimidine-based DESs

To explore the mechanism of DES formation and  $\text{SO}_2$  absorption,  $\text{C}_2\text{mimCl-7} + \text{AmPyr}$  with the highest absorption capacity was selected for FT-IR and  $^1\text{H}$  NMR analysis. In Fig. 7a, the peaks appearing at 3325 and 3161  $\text{cm}^{-1}$  are attributed to the stretching vibration of  $-\text{N}_{(\text{g})}\text{H}_2$ , the peak around 1645  $\text{cm}^{-1}$  is attributed to the bending vibration of  $-\text{N}_{(\text{g})}\text{H}_2$ , and two peaks at 1575 and 1556  $\text{cm}^{-1}$  are

attributed to the stretching vibration of the pyrimidine ring.<sup>53</sup> In DES ( $\text{C}_2\text{mimCl-7} + \text{AmPyr}$ ), the peak of  $-\text{N}_{(\text{g})}\text{H}_2$  around 1645  $\text{cm}^{-1}$  is red shifted to 1628  $\text{cm}^{-1}$ , indicating that AmPyr had hydrogen bond interactions with  $\text{C}_2\text{mimCl}$  ( $\text{N}_{(\text{g})}\text{H}\cdots\text{Cl}^-$ ). Besides, the peak of  $\text{C}_{(2)}\text{-H}$  in  $\text{C}_2\text{mimCl}$  around 3056  $\text{cm}^{-1}$  shifts to 3046  $\text{cm}^{-1}$ ,<sup>51</sup> which may be due to  $\text{Cl}^-$  forming intramolecular hydrogen bonds ( $\text{C}_{(2)}\text{-H}\cdots\text{Cl}^-$ ), leading to a decrease in force constant and vibrational energy, and a red shift in functional groups.<sup>23,29,54</sup>

For the spectrum after  $\text{SO}_2$  absorption, four new peaks attributed to  $\text{SO}_2$  could be observed. Among them, three peaks are attributed to the bending vibration (529  $\text{cm}^{-1}$ ), symmetric stretching vibration (1124  $\text{cm}^{-1}$ ), and asymmetric stretching vibration (1281  $\text{cm}^{-1}$ ) of  $\text{S}=\text{O}$ , respectively.<sup>6,22,32</sup> Compared with free  $\text{SO}_2$ , a significant red shift was observed in the stretching vibration of  $\text{S}=\text{O}$ , indicating that  $\text{Cl}^-$  in  $\text{C}_2\text{mimCl}$  may form a charge transfer interaction with S atoms in  $\text{SO}_2$  ( $\text{Cl}^-\cdots\text{SO}_2$ ).<sup>55,56</sup> Hence, the original hydrogen bonds in DESs get weakened significantly, leading to the peaks of  $-\text{C}_{(8)}\text{H}_3$ ,  $\text{C}_{(2)}\text{-H}$  and  $\text{C}_{(4+5)}\text{-H}$  shifting from 2976, 3046 and 3140  $\text{cm}^{-1}$  to 2984, 3088 and 3145  $\text{cm}^{-1}$ , respectively.<sup>32,49</sup> The fourth peak around 836  $\text{cm}^{-1}$  is attributed to the bending vibration of  $\text{S}-\text{O}$ , indicating that there exists chemical absorption of  $\text{SO}_2$ .<sup>28,57</sup> Owing to the bending vibration of  $-\text{N}_{(\text{g})}\text{H}_2$  shifting and splitting into two peaks around 1693 and 1680  $\text{cm}^{-1}$ , it is inferred that the acid-base interactions might be formed between AmPyr and  $\text{SO}_2$ .<sup>23</sup> Contrary to  $\text{SO}_2$  absorption, the FT-IR spectrum after  $\text{CO}_2$  absorption showed no significant changes compared to before absorption, indicating that there is almost no interaction between the as-prepared DESs and  $\text{CO}_2$ , thus exhibiting extremely high  $\text{SO}_2/\text{CO}_2$  selectivity.

Fig. 7b shows the  $^1\text{H}$  NMR spectra of AmPyr,  $\text{C}_2\text{mimCl}$ ,  $\text{C}_2\text{mimCl-7} + \text{AmPyr}$ , and  $\text{C}_2\text{mimCl-7} + \text{AmPyr}$  after  $\text{SO}_2$  absorption. Notably, the peak of  $-\text{N}_{(\text{g})}\text{H}_2$  shifts from 6.59 ppm in AmPyr to 6.66 ppm in DES, and the peak of  $\text{C}_{(2)}\text{-H}$  shifts from 9.70 ppm in  $\text{C}_2\text{mimCl}$  to 9.78 ppm in DES.

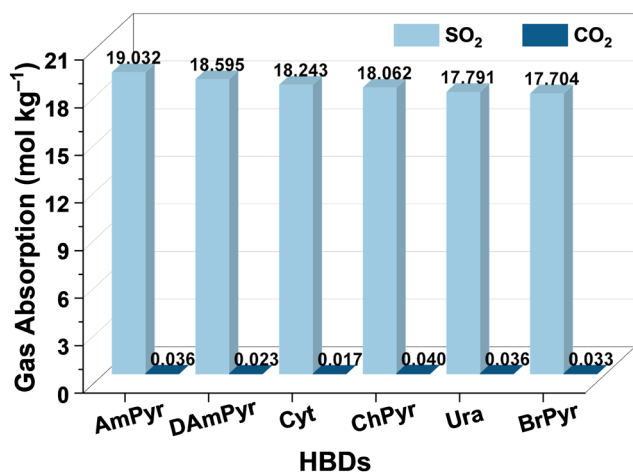


Fig. 6 The gas absorption of  $\text{C}_2\text{mimCl-7} + \text{HBDs}$ ;  $T = 298.15 \text{ K}$ ,  $P = 1.0 \text{ bar}$ .



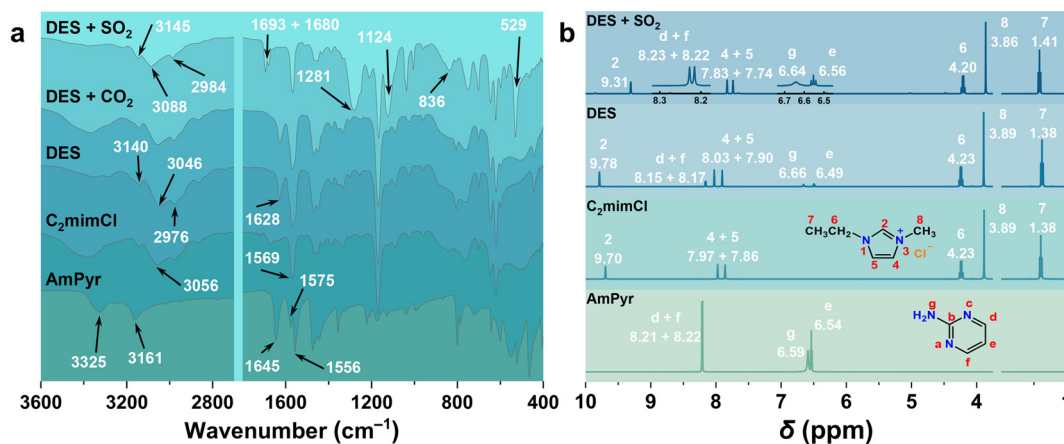


Fig. 7 (a) FT-IR spectra of  $C_2mimCl-7 + AmPyr$  after  $SO_2$  absorption (DES +  $SO_2$ ),  $C_2mimCl-7 + AmPyr$  after  $CO_2$  absorption (DES +  $CO_2$ ),  $C_2mimCl-7 + AmPyr$  (DES),  $C_2mimCl$  and  $AmPyr$ ; (b)  $^1H$  NMR spectra of DES +  $SO_2$ , DES,  $C_2mimCl$  and  $AmPyr$ .

These down-field shifts are attributed to the formation of  $N_{(g)}-H \cdots Cl^-$  and  $C_{(2)}-H \cdots Cl^-$ ,<sup>23</sup> respectively, which would reduce electron cloud density (de-shielding effect).<sup>25,58</sup> Concurrently, the peak of  $C_{(4+5)}-H$  shifts to down-field, while the peaks of  $C_{(d+f)}-H$  and  $C_{(e)}-H$  shift to up-field. In contrast, the peaks of  $C_{(2)}-H$  and  $-N_{(g)}H_2$  shift to up-field after  $SO_2$  absorption. The former is attributed to the charge transfer between the  $Cl^-$  and S atoms ( $Cl^- \cdots SO_2$ ), while the latter could be ascribed to the acid-base interaction between  $-N_{(g)}H_2$  and  $SO_2$ .<sup>25,59</sup> The shift of other C-H signals in  $C_2mimCl$  and  $AmPyr$  indicates that the original hydrogen bonds in DES have been disrupted by  $SO_2$ .

### 2.7 Regeneration of pyrimidine-based DESs

In order to avoid secondary pollution caused by a large number of waste absorbents, it is usually required that the absorbents have good regeneration performance. As shown in Fig. 8,  $C_2mimCl-7 + AmPyr$  maintains the  $SO_2$  absorption capacity of  $18.265 \text{ mol kg}^{-1}$  after 30 times of absorption-desorption. This represents excellent regeneration performance compared with the reported DESs for absorbing  $SO_2$ .<sup>16,22,23,38,60</sup> To investigate whether the

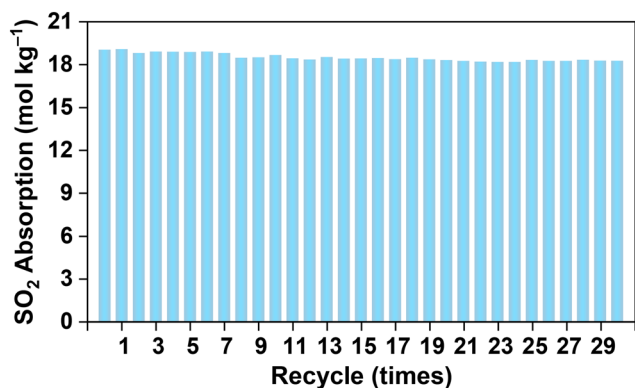


Fig. 8 The regeneration performance of  $C_2mimCl-7 + AmPyr$ .

structure of pyrimidine-based DESs is stable and maintains the original absorption performance, the  $SO_2$  absorption capacity of  $C_2mimCl-7 + AmPyr$  was measured every 7 days under the same conditions (Fig. S4). The results showed that  $C_2mimCl-7 + AmPyr$  remained liquid after 4 weeks, and maintained excellent  $SO_2$  absorption performance.

## 3 Conclusions

In this work, 14 different DESs were successfully developed and used for  $SO_2$  absorption. The density and viscosity of the as-prepared DESs show a negative correlation with temperature, but the former is linear and the latter is exponential. As the molar ratio of  $C_2mimCl$  to  $AmPyr$  increases, the  $SO_2$  absorption capacity of  $C_2mimCl-n + AmPyr$  gradually increases, ultimately reaching up to  $19.032 \text{ mol kg}^{-1}$  at  $298.15 \text{ K}$  and  $1.0 \text{ bar}$ . The thermodynamic analysis of  $SO_2$  absorption by  $C_2mimCl-7 + AmPyr$  at different temperatures was conducted using the DS-RETM equation, which not only yielded a series of thermodynamic parameters, but also successfully calculated the  $SO_2$  absorption capacity ( $19.051 \text{ mol kg}^{-1}$ ) that is highly consistent with the experimental values at  $298.15 \text{ K}$ , indicating that this model has extremely high reliability. Subsequently, it was further applied to analyze the absorption behavior of  $C_2mimCl-7 + HBDs$  DESs, and the corresponding  $m_{phys}$ ,  $m_{C_2mimCl}$ , and  $m_{HBDs}$  were obtained, demonstrating the impact of different HBDs on  $SO_2$  absorption. Dynamics analysis shows that the as-prepared DESs could reach gas-liquid equilibrium in  $40 \text{ s}$ . Besides, the present DESs exhibit remarkable  $SO_2/CO_2$  selectivity, with  $C_2mimCl-7 + AmPyr$  achieving a value as high as  $528.7$ . After 30 cycles of absorption-desorption, the  $SO_2$  absorption of the regenerated  $C_2mimCl-7 + AmPyr$  still reached  $18.265 \text{ mol kg}^{-1}$ . Finally, combining thermodynamic analysis, FT-IR, and  $^1H$  NMR results, it is indicated that the  $SO_2$  absorption process involves physical absorption and chemical absorption.



## 4 Experimental section

Preparation of DESs: C<sub>2</sub>mimCl-*n* + AmPyr DESs (*n* = 2, 3, 4, 5, 6, and 7) were prepared by combining C<sub>2</sub>mimCl and AmPyr at specified molar ratios (2:1, 3:1, 4:1, 5:1, 6:1, 7:1). The mixtures underwent heating at 353.15 K for 180 min with constant stirring. Subsequent cooling to ambient temperature yielded homogeneous liquids (Scheme S2).

C<sub>2</sub>mimCl-7 + ChPyr, C<sub>2</sub>mimCl-7 + BrPyr, C<sub>2</sub>mimCl-7 + Cyt, C<sub>2</sub>mimCl-7 + DAmPyr, C<sub>2</sub>mimCl-7 + Ura, C<sub>2</sub>mimCl-7 + AmPd and C<sub>2</sub>mimCl-7 + AmPz were prepared using 2-chloropyrimidine, 2-bromopyrimidine, 4-amino-2-hydroxypyrimidine, 4,6-diaminopyrimidine, 2,4-dihydroxypyrimidine, 3-aminopyridazine and 2-aminopyrazine as HBDs, respectively.

C<sub>2</sub>mimBr-7 + AmPyr was prepared using C<sub>2</sub>mimBr as a HBA and AmPyr as a HBD.

At a molar ratio of 7:1 and 353.15 K, with C<sub>2</sub>mimCl as a HBA and TAmPyr as a HBD, DESs could not be formed after vigorous stirring at 800 rpm for 180 min.

For other details not described, please refer to the SI.

## Conflicts of interest

There are no conflicts to declare.

## Data availability

The data that support the findings of this study are available from the corresponding author upon reasonable request.

Supplementary information (SI) is available. See DOI: <https://doi.org/10.1039/d5im00317b>.

## Acknowledgements

All authors appreciate the financial support from the National Science Foundation for Distinguished Young Scholars (No. 22425808), the National Natural Science Foundation of China (No. 22178154, 22578187), the Science Foundation of China University of Petroleum, Beijing (No. 2462022YJRC002, 2462022YJRC003), and the Carbon Neutrality Research Institute Fund (No. CNIF20240103).

## References

- W. Li, J. Li, T. D. Duong, S. A. Sapchenko, X. Han, J. D. Humby, G. F. S. Whitehead, I. J. Victórica-Yrezábal, I. da Silva, P. Manuel, M. D. Frogley, G. Cinque, M. Schröder and S. Yang, Adsorption of sulfur dioxide in Cu(II)-carboxylate framework materials: The role of ligand functionalization and open metal sites, *J. Am. Chem. Soc.*, 2022, **144**, 13196–13204.
- X. Bie, R. Wu, B. Yu, X. Quan, S. Zhang, Q. Li, Y. Zhang and H. Zhou, Deactivation mechanisms of Cu-Zn-Al<sub>2</sub>O<sub>3</sub> in CO<sub>2</sub> hydrogenation induced by SO<sub>2</sub> exposure, *Ind. Chem. Mater.*, 2025, **3**, 710–722.
- X. Cao, Y. Liu, Q. Huang, Z. Chen, J. Sun, J. Sun, S. Pang, P. Liu, W. Wang, Y. Zhang and M. Ge, Single droplet tweezer revealing the reaction mechanism of Mn(II)-catalyzed SO<sub>2</sub> oxidation, *Environ. Sci. Technol.*, 2024, **58**, 5068–5078.
- W. Zhao, J. L. Obeso, V. B. López-Cervantes, M. Bahri, E. Sánchez-González, Y. A. Amador-Sánchez, J. Ren, N. D. Browning, R. A. Peralta, G. Barcaro, S. Monti, D. Solis-Ibarra, I. A. Ibarra and D. Zhao, Achieving sub-ppm sensitivity in SO<sub>2</sub> detection with a chemically stable covalent organic framework, *Angew. Chem., Int. Ed.*, 2024, **64**, e202415088.
- W. Gong, P. Gao, Y. Gao, Y. Xie, J. Zhang, X. Tang, K. Wang, X. Wang, X. Han, Z. Chen, J. Dong and Y. Cui, Modulator-directed counterintuitive catenation control for crafting highly porous and robust metal-organic frameworks with record high SO<sub>2</sub> uptake capacity, *J. Am. Chem. Soc.*, 2024, **146**, 31807–31815.
- Q. Zhu, C. Wang, J. Yin, H. Li, W. Jiang, J. Liu, P. Li, Q. Zhang, Z. Chen and W. Zhu, Efficient and remarkable SO<sub>2</sub> capture: A discovery of imidazole-based ternary deep eutectic solvents, *J. Mol. Liq.*, 2021, **330**, 115595.
- Z. Yan, S. Y. Lai, C. L. Ngan, H. Li and A. R. Mohamed, Recent advances in energy-efficient and regenerative SO<sub>2</sub> absorption over deep eutectic solvents, *J. Environ. Chem. Eng.*, 2022, **10**, 108967.
- A. P. Abbott, G. Capper, D. L. Davies, R. K. Rasheed and V. Tambyrajah, Novel solvent properties of choline chloride/urea mixtures, *Chem. Commun.*, 2003, 70–71.
- Y. Chen and Z. Yu, Low-melting mixture solvents: Extension of deep eutectic solvents and ionic liquids for broadening green solvents and green chemistry, *Green Chem. Eng.*, 2024, **5**, 409–417.
- M. Hu, B. Han, L. Xie, B. Lu, D. Bai, N. Shi, Y. Liao, Y. Wang, L. Liu, S. Wu, R. Lan, X. Lei, C. Shi, D. Huang, Y. Li, L. Lin and J. Zhang, Ultrasonic assisted natural deep eutectic solvents as a green and efficient approach for extraction of hydroxytyrosol from olive leaves, *Ind. Chem. Mater.*, 2024, **2**, 309–320.
- Y. Chen, G. Zhao, J. Dong, J. Wang, D. Dong, Z. Li, M. Zhao, Z. Shi and Z. Niu, Green recovery of all-solid-state sodium-ion batteries/lithium-ion batteries by ionic liquids, deep eutectic solvents and low-melting mixture solvents, *Ind. Chem. Mater.*, 2025, **3**, 464–474.
- E. L. Smith, A. P. Abbott and K. S. Ryder, Deep eutectic solvents (DESs) and their applications, *Chem. Rev.*, 2014, **114**, 11060–11082.
- M. Francisco, A. van den Bruinhorst and M. C. Kroon, Low-transition-temperature mixtures (LTTMs): A new generation of designer solvents, *Angew. Chem., Int. Ed.*, 2013, **52**, 3074–3085.
- D. Yang, M. Hou, H. Ning, J. Zhang, J. Ma, G. Yang and B. Han, Efficient SO<sub>2</sub> absorption by renewable choline chloride-glycerol deep eutectic solvents, *Green Chem.*, 2013, **15**, 2261.
- D. Deng, X. Liu and B. Gao, Physicochemical properties and investigation of azole-based deep eutectic solvents as efficient and reversible SO<sub>2</sub> absorbents, *Ind. Eng. Chem. Res.*, 2017, **56**, 13850–13856.



- 16 K. Zhang, S. Ren, X. Yang, Y. Hou, W. Wu and Y. Bao, Efficient absorption of low-concentration SO<sub>2</sub> in simulated flue gas by functional deep eutectic solvents based on imidazole and its derivatives, *Chem. Eng. J.*, 2017, **327**, 128–134.
- 17 D. Lee, W. Y. Choi, K. Jang, J. Park and Y. Yoo, Functionalized imidazole–alkanolamine deep eutectic solvents with remarkable performance for low-concentration SO<sub>2</sub> absorption, *Sep. Purif. Technol.*, 2023, **307**, 122782.
- 18 X. Li, L. Meng, F. Yang, Z. Yang, J. Li, Y. Chen and X. Ji, Tuning the structure of N-methyldiethanolamine-based deep eutectic solvents for efficient and reversible SO<sub>2</sub> capture, *Chem. Commun.*, 2024, **60**, 10560–10563.
- 19 G. Long, C. Yang, X. Yang, T. Zhao, F. Liu and J. Cao, Bisazole-based deep eutectic solvents for efficient SO<sub>2</sub> absorption and conversion without any additives, *ACS Sustainable Chem. Eng.*, 2020, **8**, 2608–2613.
- 20 L. Zhang, H. Ma, G. Wei, B. Jiang, Y. Sun, X. Tantai, Z. Huang and Y. Chen, Efficient and reversible nitric oxide absorption by low-viscosity, azole-derived deep eutectic solvents, *J. Chem. Eng. Data*, 2019, **64**, 3068–3077.
- 21 Y. Chen, B. Jiang, H. Dou, L. Zhang, X. Tantai, Y. Sun and H. Zhang, Highly efficient and reversible capture of low partial pressure SO<sub>2</sub> by functional deep eutectic solvents, *Energy Fuels*, 2018, **32**, 10737–10744.
- 22 P. Zhang, G. Xu, M. Shi, Z. Wang, Z. Tu, X. Hu, X. Zhang and Y. Wu, Unexpectedly efficient absorption of low-concentration SO<sub>2</sub> with phase-transition mechanism using deep eutectic solvent consisting of tetraethylammonium chloride and imidazole, *Sep. Purif. Technol.*, 2022, **286**, 120489.
- 23 Q. Wang, H. Wu, T. Zhang, Y. Fan, W. Zhang and K. He, Efficient absorption of low partial pressure SO<sub>2</sub> by deep eutectic solvents based on pyridine derivatives, *Chem. Eng. Res. Des.*, 2022, **177**, 36–44.
- 24 Z. Wang and D. Yang, SO<sub>2</sub> capture by 2-pyridineethanol through the formation of a zwitterionic liquid, *Chem. Commun.*, 2022, **58**, 6212–6214.
- 25 C. Wang, H. Wu, J. Li, J. Zhang, J. Zhang, J. Ding, H. Li, H. Li and W. Zhu, Surpassingly efficient, selective, and reversible absorption of SO<sub>2</sub> through pyridine based deep eutectic solvents, *Chem. Eng. J.*, 2023, **471**, 144394.
- 26 T. Yang, Y. Wang, Z. Huang, F. Liu, Q. Liao and T. Zhao, Deep eutectic solvents composed of 1-methyl-3-ethylimidazole halides and pyridine derivatives for efficient absorption and conversion of SO<sub>2</sub> into cyclic sulfites under ambient conditions, *Sep. Purif. Technol.*, 2025, **361**, 131475.
- 27 P. Zhang, Z. Tu, X. Zhang, X. Hu and Y. Wu, Acidic protic ionic liquid-based deep eutectic solvents capturing SO<sub>2</sub> with low enthalpy changes, *AIChE J.*, 2023, **69**, e18145.
- 28 Y. Zou, C. Wang, H. Ji, P. Wu, Y. Chao, X. Yu, Z. Yu, H. Liu, Z. Liu and W. Zhu, Rapid, selectivity, and reversibility absorption of SO<sub>2</sub> via purine-based deep eutectic solvents and thermodynamic analysis, *Green Chem. Eng.*, 2026, **7**, 180–190.
- 29 P. Li, X. Wang, T. Zhao, C. Yang, X. Wang and F. Liu, Deep eutectic solvents formed by EmimCl plus lactams: Effective SO<sub>2</sub> capture and conversion into sulphur via DESs-mediated claus process, *Chem. Eng. J.*, 2021, **422**, 130033.
- 30 X. Y. Luo, X. Fan, G. L. Shi, H. R. Li and C. M. Wang, Decreasing the viscosity in CO<sub>2</sub> capture by amino-functionalized ionic liquids through the formation of intramolecular hydrogen bond, *J. Phys. Chem. B*, 2016, **120**, 2807–2813.
- 31 M. Pan, Y. Zhao, X. Zeng and J. Zou, Efficient absorption of CO<sub>2</sub> by introduction of intramolecular hydrogen bonding in chiral amino acid ionic liquids, *Energy Fuels*, 2018, **32**, 6130–6135.
- 32 K. Sheng, D. Li and Y. Kang, Unexpectedly promoted SO<sub>2</sub> capture in novel ionic liquid-based eutectic solvents: The synergistic interactions, *J. Mol. Liq.*, 2021, **337**, 116432.
- 33 Y. Cao, J. Zhang, Y. Ma, W. Wu, K. Huang and L. Jiang, Designing low-viscosity deep eutectic solvents with multiple weak-acidic groups for ammonia separation, *ACS Sustainable Chem. Eng.*, 2021, **9**, 7352–7360.
- 34 G. Long, C. Yang, X. Yang, T. Zhao and M. Xu, Deep eutectic solvents consisting of 1-ethyl-3-methylimidazolium chloride and glycerol derivatives for highly efficient and reversible SO<sub>2</sub> capture, *J. Mol. Liq.*, 2020, **302**, 112538.
- 35 B. Jiang, H. Zhang, L. Zhang, N. Zhang, Z. Huang, Y. Chen, Y. Sun and X. Tantai, Novel deep eutectic solvents for highly efficient and reversible absorption of SO<sub>2</sub> by preorganization strategy, *ACS Sustainable Chem. Eng.*, 2019, **7**, 8347–8357.
- 36 X. Wu, R. Guan, W. Zheng and K. Huang, New deep eutectic solvents formed by 1-ethyl-3-methylimidazolium chloride and dicyandiamide: Physicochemical properties and SO<sub>2</sub> absorption performance, *J. Taiwan Inst. Chem. Eng.*, 2021, **119**, 45–51.
- 37 D. Deng, G. Han and Y. Jiang, Investigation of a deep eutectic solvent formed by levulinic acid with quaternary ammonium salt as an efficient SO<sub>2</sub> absorbent, *New J. Chem.*, 2015, **39**, 8158–8164.
- 38 C. Wang, G. Cui, X. Luo, Y. Xu, H. Li and S. Dai, Highly efficient and reversible SO<sub>2</sub> capture by tunable azole-based ionic liquids through multiple-site chemical absorption, *J. Am. Chem. Soc.*, 2011, **133**, 11916–11919.
- 39 Y. Jiang, X. Liu and D. Deng, Solubility and thermodynamic properties of SO<sub>2</sub> in three low volatile urea derivatives, *J. Chem. Thermodyn.*, 2016, **101**, 12–18.
- 40 D. Yang, Y. Han, H. Qi, Y. Wang and S. Dai, Efficient absorption of SO<sub>2</sub> by EmimCl-EG deep eutectic solvents, *ACS Sustainable Chem. Eng.*, 2017, **5**, 6382–6386.
- 41 K. Zhang, S. Ren, Y. Hou and W. Wu, Efficient absorption of SO<sub>2</sub> with low-partial pressures by environmentally benign functional deep eutectic solvents, *J. Hazard. Mater.*, 2017, **324**, 457–463.
- 42 G. Cui, J. Liu, S. Lyu, H. Wang, Z. Li and J. Wang, Efficient and reversible SO<sub>2</sub> absorption by environmentally friendly task-specific deep eutectic solvents of PPZBr + Gly, *ACS Sustainable Chem. Eng.*, 2019, **7**, 14236–14246.
- 43 Z.-M. Li, W.-Q. Gong, J.-F. Li, S.-X. Zhu, D.-J. Tao and Y. Zhou, Efficient and selective absorption of SO<sub>2</sub> by low-



- viscosity matrine-based deep eutectic solvents, *J. Mol. Liq.*, 2022, **367**, 120521.
- 44 Y. Zhao, J. Dou, R. Dai, H. Bai, S. Khoshk Rish, X. Xiao and J. Yu, Superefficient absorption of low-concentration SO<sub>2</sub> in flue gas using new ternary imidazole-based deep eutectic solvents: Mechanism, thermodynamics, and process analysis, *Energy Fuels*, 2022, **36**, 8351–8359.
- 45 Y. Zhao, J. Dou, H. Li, R. Dai, H. Bai, S. Khoshk Rish, X. Chen, X. Xiao and J. Yu, Low-cost Na<sub>2</sub>S-EG-MTPB deep eutectic solvents absorb SO<sub>2</sub> effectively at a high temperature in flue gas, *Sep. Purif. Technol.*, 2022, **303**, 122283.
- 46 T. Zhou, Y. Zhao, X. Xiao, Y. Liu, H. Bai, X. Chen, J. Dou and J. Yu, Effective absorption mechanism of SO<sub>2</sub> and NO<sub>2</sub> in the flue gas by ammonium-bromide-based deep eutectic solvents, *ACS Omega*, 2022, **7**, 29171–29180.
- 47 W. J. Jiang, F. Y. Zhong, L. S. Zhou, H. L. Peng, J. P. Fan and K. Huang, Chemical dual-site capture of NH<sub>3</sub> by unprecedentedly low-viscosity deep eutectic solvents, *Chem. Commun.*, 2020, **56**, 2399–2402.
- 48 P. Liu, K. Cai, X. Zhang, X. Wang, M. Xu, F. Liu and T. Zhao, Rich ether-based protic ionic liquids with low viscosity for selective absorption of SO<sub>2</sub> through multisite interaction, *Ind. Eng. Chem. Res.*, 2022, **61**, 5971–5983.
- 49 D. Yang, S. Zhang, D. E. Jjiang and S. Dai, SO<sub>2</sub> absorption in EmimCl-TEG deep eutectic solvents, *Phys. Chem. Chem. Phys.*, 2018, **20**, 15168–15173.
- 50 T. Zhao, J. Liang, Y. Zhang, Y. Wu and X. Hu, Unexpectedly efficient SO<sub>2</sub> capture and conversion to sulfur in novel imidazole-based deep eutectic solvents, *Chem. Commun.*, 2018, **54**, 8964–8967.
- 51 M. Lv, D. Yang and J. Chen, Deep eutectic solvents consisting of 1-ethyl-3-methylimidazolium chloride and biobased 2-pyrrolidone for reversible SO<sub>2</sub> capture, *ChemistrySelect*, 2020, **5**, 7142–7147.
- 52 H. Wang, P. Wu, C. Li, J. Zhang and R. Deng, Reversible and efficient absorption of SO<sub>2</sub> with natural amino acid aqueous solutions: Performance and mechanism, *ACS Sustainable Chem. Eng.*, 2022, **10**, 4451–4461.
- 53 S. Akyüz and T. Akyüz, FT-IR spectroscopic investigations of surface and intercalated 2-aminopyrimidine adsorbed on sepiolite and montmorillonite from Anatolia, *J. Mol. Struct.*, 2003, **651–653**, 205–210.
- 54 C. Wang, Q. Bi, Y. Huo, Z. Zhang, D. Tao, Y. Shen, Q. Zhu, Z. Chen, H. Li and W. Zhu, Investigation of amine-based ternary deep eutectic solvents for efficient, rapid, and reversible SO<sub>2</sub> absorption, *Energy Fuels*, 2021, **35**, 20406–20410.
- 55 X. Yang, Y. Zhang, F. Liu, P. Chen, T. Zhao and Y. Wu, Deep eutectic solvents consisting of EmimCl and amides: Highly efficient SO<sub>2</sub> absorption and conversion, *Sep. Purif. Technol.*, 2020, **250**, 117273.
- 56 K.-Y. Lee, C.-S. Kim, H.-G. Kim, M.-S. Cheong, D. K. Mukherjee and K.-D. Jung, Effects of halide anions to absorb SO<sub>2</sub> in ionic liquids, *Bull. Korean Chem. Soc.*, 2010, **31**, 1937–1940.
- 57 Z. L. Li, L. S. Zhou, Y. H. Wei, H. L. Peng and K. Huang, Highly efficient, reversible, and selective absorption of SO<sub>2</sub> in 1-ethyl-3-methylimidazolium chloride plus imidazole deep eutectic solvents, *Ind. Eng. Chem. Res.*, 2020, **59**, 13696–13705.
- 58 W. S. Ham, H. Choi, J. Zhang, D. Kim and S. Chang, C<sub>2</sub>-selective, functional-group-divergent amination of pyrimidines by enthalpy-controlled nucleophilic functionalization, *J. Am. Chem. Soc.*, 2022, **144**, 2885–2892.
- 59 C. Wang, J. Zhang, Y. Zou, J. Ding, H. Li, M. Zhang, H. Li and W. Zhu, Effects of attractive electrostatic interactions on sulfur dioxide capture by functionalized deep eutectic solvents with abundant negative sites, *Chem. Eng. J.*, 2025, **519**, 165030.
- 60 S. Sun, Y. Niu, Q. Xu, Z. Sun and X. Wei, Efficient SO<sub>2</sub> absorptions by four kinds of deep eutectic solvents based on choline chloride, *Ind. Eng. Chem. Res.*, 2015, **54**, 8019–8024.

